Full length article

Direct measurement of the direction-dependent mechanical behaviour of skeletal muscle extracellular matrix

Stephan Kohn[a], Kay Leichsenring[a], Ramachandra Kuravi[b,c], Alexander E. Ehret[b,c], Markus Böl[a,*]

[a] Institute of Mechanics and Adaptronics, Technische Universität Braunschweig, Braunschweig D-38106, Germany
[b] Empa, Swiss Federal Laboratories for Materials Science and Technology, Dübendorf CH-8600, Switzerland
[c] Institute for Mechanical Systems, ETH Zurich, Zürich CH-8092, Switzerland

A B S T R A C T

This paper reports the first comprehensive data set on the anisotropic mechanical properties of isolated endo- and perimysial extracellular matrix of skeletal muscle, and presents the corresponding protocols for preparing and testing the samples. In particular, decellularisation of porcine skeletal muscle is achieved with caustic soda solution, and mechanical parameters are defined based on compressive and tensile testing in order to identify the optimal treatment time such that muscle fibres are dissolved whereas the extracellular matrix remains largely intact and mechanically functional. At around 18 h, a time window was found and confirmed by histology, in which axial tensile experiments were performed to characterise the direction-dependent mechanical response of the extracellular matrix samples, and the effect of lateral pre-compression was studied. The typical, large variability in the experimental stress response could be largely reduced by varying a single scalar factor, which was attributed to the variation of the fraction of extracellular matrix within the tissue. While experimental results on the mechanical properties of intact muscle tissue and single muscle fibres are increasingly available in literature, there is a lack of information on the properties of the collagenous components of skeletal muscle. The present work aims at closing this gap and thus contributes to an improved understanding of the mechanics of skeletal muscle tissue and provides a missing piece of information for the development of corresponding constitutive and computational models.

Statement of significance

This article reports the first comprehensive data set on the anisotropic mechanical properties of isolated endo- and perimysial extracellular matrix of skeletal muscle, and presents the corresponding protocols for preparing and testing the samples. On the one hand, the results of this study contribute to the understanding of muscle mechanics and thus to understanding of load transfer mechanisms inside the muscle tissue. On the other hand, these results are relevant to the fields of constitutive formulation of muscle tissue and tissue-engineering grafts.

1. Introduction

Probably more prominent than any other organ, skeletal muscle is characterised by a strongly hierarchical structure, in which muscle fibres are surrounded by an intricately organised extracellular matrix (ECM). The ECM of skeletal muscle is categorised into three sub-classes: The endomysium envelopes the single muscle fibres, the perimysium groups muscle fibres into fascicles, and the epimysium surrounds the whole muscle. Here, we focus on the endo- and perimysium within the muscle tissue. Composed of collagen fibre types I, III, IV, VI, and XII [e.g. 1,2], the endomysium represents up to 1.2% of the muscle dry weight [3]. It embeds the muscle fibres in a honeycomb-like structure [e.g. 4–6], whose thin walls are formed by a random network of distributed collagen fibres. Due

to its location next to the actively contracting muscle fibres, the endomysium plays an important role for lateral force transmission [3,7]. The perimysium reaches up to 4.6% of muscle dry weight [3]. The collagen fibres within the perimysium vary in composition but contain a great amount of collagen type I and, to a smaller extent, types III, VI, and XII [1,2]. In contrast to the endomysium the collagen network of the perimysium shows four hierarchical levels of organisation that seem to play a major role in force transmission [8]: (i) A regular lattice of interwoven longitudinal and angled circumferential fibres, (ii) a collagen plexus where circumferential fibres meet, (iii) a sub-plexus at each end of the lattice branches, and (iv) an arrangement of tubes composed of collagen cables connecting the tendons, see also [8–11].

The ECM plays an important role for muscle tissue integrity and functionality [8–12], despite its comparatively low content within the tissue, which amounts to only 1-10% of muscle dry weight [13]. It provides mechanical support for nerves and vessels, gives structure to the muscle fibres during contraction, contributes in transmitting forces from the muscle fibre to the tendon, and furnishes the muscle tissue with elasticity. In addition to this load-transmitting function of the ECM, advances in cell as well as molecular biology and genetics continuously provide new insights, indicating that ECM is also significantly involved in signaling [14–17]. The ECM of soft biological tissues undergoes continuous remodelling both in healthy and diseased conditions, accompanied by changes in composition and structure [18,19]. Since these alterations can heavily affect organ function [e.g. 20–26], it is not surprising that the composition, structure, and properties of ECM are also associated with medical questions [e.g. 27,28].

While the analysis of the microstructure of muscle ECM has been well established due to advances in microscopy and staining techniques, studies on the mechanical characteristics of ECM are very rare. Due to their relatively simple realisation, the vast majority of studies focus on the experimental characterisation of the mechanical behaviour of dissected muscle tissue samples, i.e., of the composite of ECM and fibres. Typically, mechanical characterisation is performed through, e.g., unconfined compression [29–38], semi-confined compression [39,40], axial tension [33,36,38,41–50], and shear [33,51]. On the one hand, these studies are used to understand the muscle tissue's macroscopic mechanical behaviour, and on the other hand, to identify material parameters for constitutive material models. However, the results of these experiments can only deliver 'averaged' responses of the composite and hardly allow estimating the contribution of the ECM.

Even though the small dimensions of the ECM layers and their disposition within the muscle tissue render ECM-specific measurements very demanding, there exist a few recent approaches towards this goal: An indirect method to characterise ECM was presented based on the difference between the mechanical responses of single muscle fibres and a fascicle [52–55]. The authors determined stress-length/strain relations of single muscle fibres, muscle fascicles (connected by ECM), and groups of unconnected fibres. The comparison of the mechanical responses of the different fibres and fascicles allows to estimate the mechanical characteristics of the ECM. Although generally depending on species and age, these studies demonstrated that the ECM typically exhibits highly non-linear behaviour, and gains higher stiffness than the muscle fibres. A direct method is based on decellularisation, more precisely, on removing everything but ECM from the tissue by combining physical, chemical, and enzymatic processes [e.g. 56–60]. At the end of these processes, the ECM is available for mechanical testing. In this way, Gillies et al. [61] realised tension experiments on ECM samples of murine tibialis anterior muscle fascicles and found non-linear, exponential-like stress-strain characteristics. Noteworthy, in comparison to the endo- and perimysium the separation of the epimysial layer from the muscle is simpler, and the mechan-

ical behaviour can be characterised by applying standard testing methods [4,62], revealing an exponential-type tensile stress-strain response typical for soft collagenous tissues.

To the best of our knowledge, there exist currently no systematic experimental study to determine the anisotropic mechanical behaviour of skeletal muscle ECM. The central goal of the present work is to establish a better understanding of the ECM mechanical characteristics through axial tension experiments on decellularised and non-decellularised strips of skeletal muscle. It is known that caustic soda, i.e., sodium hydroxide solution (NaOH) can be used to decellularise the muscle fibres from the muscle tissue [4,61,63–65]. For mechanical testing, it needs to be assured that this treatment effectively removes muscle fibres but does not significantly affect the structure and properties of the ECM. Accordingly, a protocol for the preparation of decellularised tissue samples suitable for mechanical characterisation is developed and proposed in the present work. Moreover, we study the effect of transversely compressing the decellularised samples by varying extents. We show that this operation could serve as an indicator for successful cell removal and, in addition, it provides insight to the anisotropy of the ECM, since the forced compaction generates quasi-planar structures.

The outcome of this study will help filling the existing gap of knowledge with regard to the mechanics of skeletal muscle ECM. It will allow the identification of the ECM's material characteristics necessary to establish multi-scale models, see Kuravi et al. [66], and contribute to an enhanced understanding of load transfer mechanisms in muscle tissue. The paper is organised as follows: A description of the experimental methods and the corresponding results are provided in Sections 2 and 3, respectively, followed by a critical discussion in Section 4 and concluding remarks in Section 5.

2. Materials and methods

2.1. Ethical approval

The study was exempted from ethical committee review according to national regulations (German Animal Welfare Act), as muscles from healthy, female domestic pigs were obtained from a slaughterhouse immediately after animal sacrifice.

2.2. Tissue sample dissection and processing

Hind legs of six ($n = 6$) female domestic pigs (*Sus scrofa domestica*, age: ~6 month, mass: ~90 to 100 kg, one leg per animal) were obtained from a slaughterhouse immediately after animal sacrifice. After transport in a cooling box to the laboratory, biceps femoris muscles were excised and stored at 4 °C in a climatic chamber wrapped in Dulbecco's phosphate buffered saline (DPBS) soaked cloths. Following Table 1, tissue samples ($n = 246$) with length, width, and thickness approximately 60, 8, and 4 mm, respectively, were cut in dependence on their fibre orientation (0°, 45°, 90°) to realise tension and compression experiments. Alginate was used to stabilise the tissue during cutting with a utility cutter [39]. Before performing mechanical tests, the differently processed tissue samples were divided into 3 groups ($G_{1/2/3}$).

As a reference, G_1 comprises the fresh, untreated tissue samples, which were cut out of the muscle at different angles (0°, 45°, 90°) with respect to the gross direction of the muscle fibres observable in the tissue. After cutting the samples, they were stored at 4 °C in a climatic chamber, wrapped in DPBS-soaked cloths. Sampling of fresh specimens was completed within 6 h of animal sacrifice.

In order to determine the optimal time t^* such that all muscle cells are effectively dissolved by the NaOH solution while the mechanical properties of the ECM are not significantly affected, the

Table 1
Tension and compression experiments conducted within this study.

Group	Level of pre-compression [%]		Untreated 0°	45°	90°	NaOH-treated 0°	45°	90°
G_1	0	tension	5	5	5	–	–	–
G_2	0	tension	–	–	–	73	–	–
		compression	–	–	–	93	–	–
G_3	0		–	–	–	6	7	10
	45	tension	–	–	–	5	7	12
	90		–	–	–	6	6	6

Table 2
Overview of the test group G_2 performed within this study.

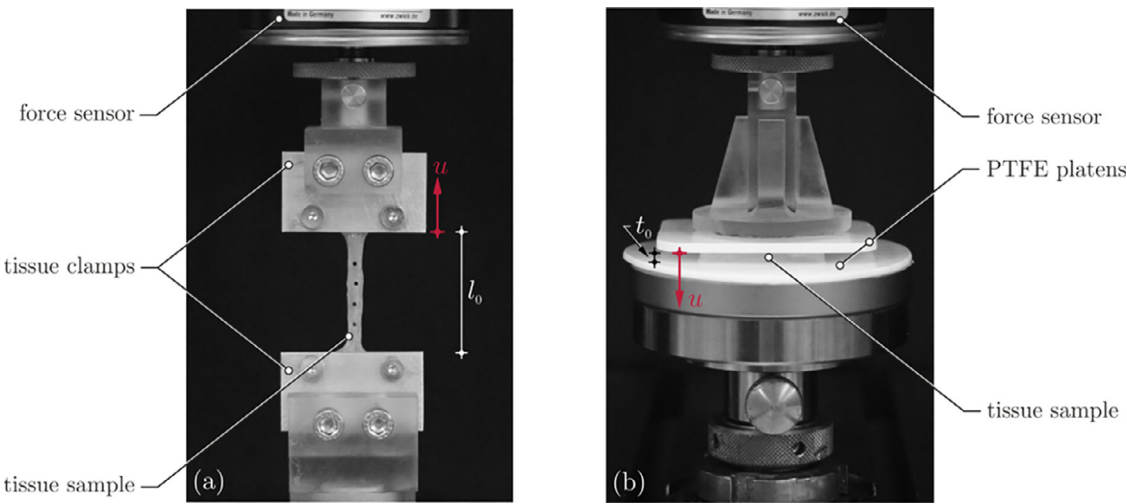| Group		Time of insertion into NaOH solution [h] 6	9	12	15	18	21	24	27	30	33	36
G_2	tension	8	8	8	8	8	6	8	7	6	4	2
	compression	8	11	7	6	12	8	12	8	9	8	4

Fig. 1. Setup for (a) axial tension and (b) transversal compression experiments.

tissue samples of G_2 were placed in 3% NaOH solution for different time periods, see Table 2. Tissue samples were cut along the visually perceivable 'gross' muscle fibre direction (0°), then weighed and finally placed in 100 ml NaOH solution per sample. After reaching the aimed time period listed in Table 2, the samples were removed from the NaOH solution and placed for 45 min in DPBS solution (125 ml solution per sample) and thereafter again in fresh DPBS solution (125 ml solution per sample) for another 15 min. Before the samples were finally weighed and subjected to mechanical testing, they were again stored in DPBS-soaked cloths at 4 °C in the climatic chamber. After determining the optimal time period for decellularisation t^*, see Section 3.2, a third group of tissue samples (G_3) was prepared from tissue samples oriented at 0°, 45°, and 90°, following the protocol for the G_2-samples for the defined time t^*. To ensure that the time lapse between dissolving, rinsing, and testing of the samples was approximately constant, 4-5 samples were successively inserted in NaOH every hour, respectively. From a few tissue samples, inserted for 0, 12, and 18 h, histological sections were prepared and stained with Picro-Sirius red, see Appendix A.

2.3. Tissue strip experiments

All axial tension and transversal compression experiments were conducted with two axial testing machines (Zwick Z0.5, Zwick GmbH & Co. Ulm, Germany), cf. Fig. 1, equipped with 5 N (tension) and 10 N (compression) load cells.

2.3.1. Transversal compression experiments

Cuboid samples ($n = 93$, see Table 1), treated with NaOH solution, were subjected to transversal compression prior to tensile testing, see Fig. 1(b). The experiments were performed up to either 45% ($n = 24$) or 90% ($n = 18$) nominal compressive strain ε at a rate of $\dot{\varepsilon} = 0.5\%$ s^{-1} in line with our former protocols [39,40,67]. While the displacement u of the upper platen was predefined, the resulting force F was measured and converted to mean engineering stress via $P = F/A_{\text{trans}}$ by division through the transversal cross-sectional area A_{trans}, measured from a digital image which was recorded before testing. The transversal compressive stretch $\lambda_{\text{trans}} = 1 + \varepsilon = 1 + u/t_0$ was calculated from u and the undeformed sample thickness t_0, cf. Fig. 1(b). In order to diminish friction effects, the polytetrafluoroethylene (PTFE) platens were sprayed with silicon oil for lubrication [68]. After transversal compression of the samples they were transferred to the second testing machine to perform the axial tension experiments, see Section 2.3.2.

2.3.2. Axial tension experiments

Before performing the axial tensile experiments on untreated and NaOH-treated tissue samples, the cross-section area A_{ten} of each of the strips was quantified by means of digital images. The
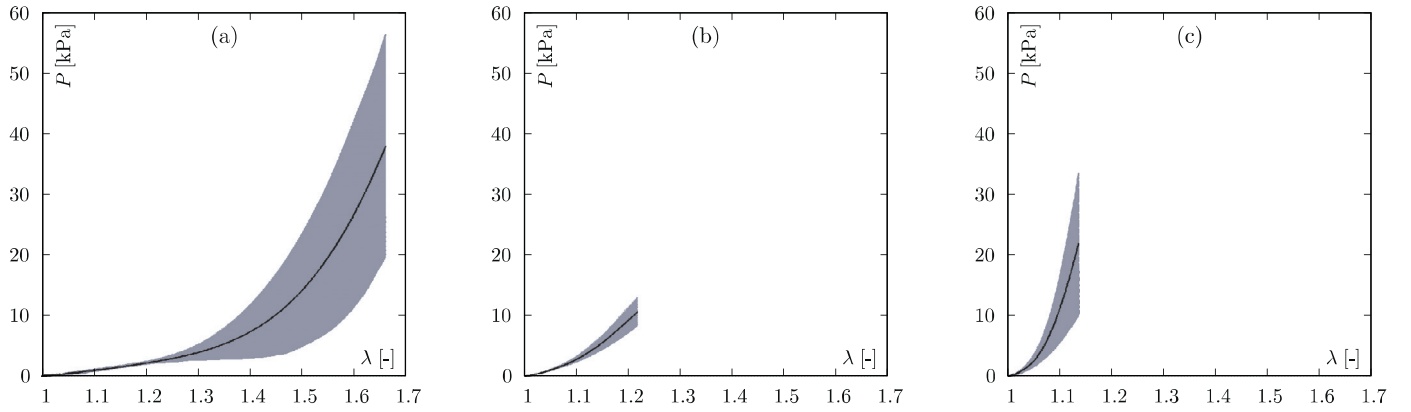
Fig. 2. Tensile stress-stretch responses of fresh muscle samples ($n = 15$), c.f. Table 1, for loading directions of (a) $0°$, (b) $45°$, and (c) $90°$ with respect to the tissues' fibre direction. Solid curves indicate mean values whereas shaded areas depict the standard deviations. Note, the unprocessed raw data can be found in the supplementary material, see Section 6.

strips, either pristine or compressed transversally before by 45% or 90%, were then fixed in clamps covered with sandpaper to reduce tissue slippage, see Fig. 1(a). The axial tension experiments were performed at a nominal strain rate of $\dot{\varepsilon} = 0.5\%\ \text{s}^{-1}$ up to failure of the strips. While the displacement u of the upper clamp was specified, the resulting force F was measured and converted to mean engineering stress as $P = F/A_{\text{ten}}$ by division through the undeformed cross-sectional area A_{ten}. The axial stretch $\lambda_{\text{trans}} = 1 + u/l_0$ was calculated from u and the undeformed sample length l_0, cf. Fig. 1(a). For treated sample an additional stress P_{ECM} was introduced by referring the force to an estimate of the ECM fraction ϕ of the sample, taken as 10%, cf. Kjaer [13] and Gillies and Lieber [11].

2.4. Data processing

The experimental raw data in form of force and displacement include up to 18,000 measuring points for both, the elastic and failure region. In order to make the data manageable all raw data underwent three processing steps: First, all data were smoothed, and the number of data points was reduced to a maximum of 100. Secondly, the reference state was associated with a small preforce, that differed between the fresh (muscle) and treated (ECM) samples in order to achieve comparable pre-stress. For untreated samples a force of 30 mN was chosen, corresponding to about 0.7 kPa pre-stress, depending on the exact dimensions of a specimen, and comparable to the pre-load used in Takaza et al. [48]. Taking into account that the ECM amount of skeletal muscles is around 10% of the dry weight, and assuming that it takes an approximately 10%-fraction of the tissue cross-section, 3 mN was selected for the chemically treated samples to facilitate comparability of the results, so that the threshold force per effective material cross-section agree. We note that these pre-loads were subtracted from the stress when plotting the results unless stated otherwise. Note, the unprocessed raw data (Figs. 2 and 5) can be found in the supplementary material, see Section 6. Finally, the elastic regions of the force-displacement curves were determined by successively computing tangents $\mathcal{T}_i$ by finite differences at the points u_i, $i = 1, 2, \ldots, m$, where m indicates the maximum number of measuring points. The elastic range of the curve is defined as the region where the slope is monotonically increasing, i.e., where $\mathcal{T}_{i+1} \geq \mathcal{T}_i$. The point u_j at which $\mathcal{T}_{j+1} < \mathcal{T}_j$ marks the end point of the elastic region. Apart from this, measurements were discarded from the analysis if they could not be evaluated due to operational disturbances (e.g. slipping of the specimen under compression or unintentional shift of the camera) and tearing of the specimens in the clamping region during tensile experiments.

2.5. Superposition of muscle fibre and ECM responses

The here obtained data on decellularised tissue samples was combined with previous results on porcine biceps femoris muscle fibres [69] in order to investigate whether the passive response of skeletal muscle can be calculated by adding the responses of ECM and muscle fibres according to a simple rule of mixtures. This analysis is important with regard to the development of mechanical models of the tissue, in which muscle fibres and ECM are commonly assumed in a parallel arrangement. To this end, it is assumed that along the gross muscle fibre direction, ECM and fibres are homogenously distributed, so that the volume fraction coincides with its fraction ϕ of the cross-sectional area A_{ten} of samples cut along that direction ($0°$). If muscle fibres and ECM respond to a tensile load with a characteristic force per unit area P_{ECM} and P_{MF}, respectively, the mean nominal stress of $0°$ fresh muscle samples should calculate as

$$\bar{P}_{\text{fresh}}(\lambda) = \bar{\phi}\bar{P}_{\text{ECM}}(\lambda) + (1 - \bar{\phi})\bar{P}_{\text{MF}}(\lambda) = \bar{P}_{\text{decell}}(\lambda) + (1 - \bar{\phi})\bar{P}_{\text{MF}}(\lambda), \tag{1}$$

where the overline indicates the mean and $\bar{P}_{\text{decell}}$ is the nominal stress obtained when referring to the force obtained from the decellullarised, treated samples to A_{ten}. However, the ansatz in Eq. (1) assumes that ECM and muscle fibres are composed in a configuration that corresponds to the reference state used in mechanical testing, and that they experience the same longitudinal stretch λ in the composite tissue, equal to the tissue stretch. To shed light on this issue, we compose ECM and muscle fibres at a reference state that corresponds to small pre-loads, 3 mN and 1 μN respectively, defined through the resolution of the test set-ups. It is assumed that differences in the effective stretch of the components can result from (i) a mismatch in these configurations but also (ii) relative deformations between the components caused by structural effects, such as the alignment or straightening of undulations. We thus posed the question, what stretch λ_{MF} a muscle fibre should experience within the tissue so that the response of composite and fresh tissue are in agreement. To this end, the actual response of single muscle fibres from Böl et al. [69] was interpolated to obtain $P_{\text{MF}} = g(\lambda_{\text{MF}})$, and λ_{MF} was determined numerically such that this matches the difference between the stresses in fresh and decellularised tissue, i.e., $(1 - \phi)g(\lambda_{\text{MF}}) = \bar{P}_{\text{fresh}}(\lambda) - \bar{P}_{\text{decell}}(\lambda)$.

2.6. Normalisation of tensile stress response

After removal of the muscle fibres, the force per area of the undeformed tissue is given by $P = P_{\text{decell}} = \phi P_{\text{ECM}}$. Hypothesising

that the variability between the individual samples (k) is mainly caused by the variation in ECM content [70,71] a specimen-specific normalisation factor f was determined, that characterises the deviation from the mean response $\bar{P}$. To this end, it was hypothesised that for each specimen k there exists a factor $f = f_k$, so that the difference between the mean response $\bar{P}$ and the weighted sample-specific response $f_k P^{(k)}$ is minimised. For each set of force-displacement data the individual factor f_k was obtained by minimising the objective function

$$\mathcal{O}(f_k) = \frac{1}{m} \sum_{i=1}^{m} \sqrt{\left(\bar{P}_i - f_k P_i^{(k)}\right)^2}, \qquad (2)$$

where m represents the number of data points in the mean curve.

2.7. Statistics

In order to define the optimal insertion time of the samples in 3% NaOH necessary for decellularisation, see Appendix B, and to determine whether or not the fibre orientation of the fresh (Fig. 2) and NaOH-treated tissues (Fig. 5) have a significant effect on the stress-stretch response during tension, the data were analysed statistically. To this end, Kolmogorov–Smirnov test with Lilliefors correction showed non-normal distribution of the data. Consequently, unpaired Mann-Whitney U-tests were performed on the stress values of transversal compression and axial tension experiments on treated specimens between 6 and 30 h. Additionally, Mann–Whitney U-tests were executed on the stress values of three fibre orientations at each given discretised value of the stretch λ, respectively. We tested for the null hypothesis that the mean values of the measured stress values of the two groups are equal at a significance level of $\alpha = 0.05$.

3. Results

3.1. Axial tension experiments on fresh tissue samples

Fig. 2 shows the results of the orientation-dependent tension experiments (group G_1) in form of mean stress-stretch curves and standard deviation for the elastic region. Note that in order to provide mean values and standard deviations from all samples, the stretch range shown in Fig. 2 corresponds to the smallest elastic region of the tested samples.

Independent of the fibre orientation all curves are characterised by a clearly non-linear material response. The stiffest material response is provided by tissue samples in which the fibres are aligned perpendicular to the direction of loading, cf. Fig. 2(c). Tissue samples with $45°$ oriented fibres (b) provide the second stiffest response, followed by the samples with fibres oriented parallel to the direction of loading, see (a). This is also documented in Table 3, where the secant stiffnesses $K_{\lambda=1.09} = \Delta P / \Delta \lambda$ are shown. The value of $\lambda = 1.09$ was selected for the sake of comparability since it marks the maximum stretch in the smallest elastic region among all tested treated and untreated samples. Further,

Table 3
Mean and standard deviation of maximum stress P_{max} and stretch λ_{max}. Note, the index 'max' indicated the end value of the material responses' elastic range. Note, a discussion of the relativ high maximum stretch of 1.9 in fibre direction is included in Section 4.1. Further, $K_{\lambda=1.09}$ denotes the secant stiffness, evaluated at the stretch value $\lambda = 1.09$.

	0°	45°	90°
P_{max} [kPa]	100.0 ± 24.0	13.9 ± 3.0	32.6 ± 18.7
λ_{max} []	1.9 ± 0.1	1.3 ± 0.0	1.2 ± 0.0
$K_{\lambda=1.09}$ [kPa]	9.4	27.0	100.9

Table 3 shows the maximum stresses and stretches in the form of mean values and standard deviations.

While with increasing degree of fibre orientation the maximum stretch decreases, the maximum stress is reached for the 0° samples, followed by 90° and 45° samples, respectively. With respect to Fig. 2, the stretches indicating the end points of the elastic regions reduce from 1.66 (0°) over 1.22 (45°) to 1.14 (90°). However, performing Mann–Whitney U-tests, see Section 2.7, show that all three stress-strain curves (0°, 45°, 90°) are significantly different from each other, emphasising that the different fibre orientations have a significant influence on the stress-strain responses.

3.2. Mechanical experiments for the determination of the optimal insertion time t^*

An essential issue of this study is the determination of the point in time at which the muscle fibres of the tissue samples inserted in 3% NaOH solution were dissolved, but the ECM is still physically intact. It is assumed that at this time point, the muscle fibres have completely dissolved and can be pressed out of the ECM structure like a liquid with low mechanical effort. At that instant the ECM structure is still expected to be mechanically intact, and to withstand tensile loads. Therefore, two load states were applied to subsets of the samples after subjecting them to NaOH solution for different periods of time: On the one hand, transversal compression experiments ($n = 93$) were carried out to push the dissolved cell remainders out of the ECM scaffold, and on the other hand, longitudinal tensile experiments ($n = 73$) were performed to test for the integrity of the ECM at that instant of time. In order to compare the results from different treatment times, a criterion was needed, and to this end, the mechanical stress and the tangent at the end of the elastic range were evaluated. In Fig. 3 the maximum elastic stress, (a) and (b), and the tangent at this point, (c) and (d), is represented against the duration of the NaOH treatment.

As principally expected, both, the stresses (upper row) and the tangent (lower row) decrease with increasing insertion time. Independent of the load state, the course of the two metrics can be roughly divided into three regions (I, II, III). The middle region (II) is characterised by approximately constant characteristics, and spans from around 15 to 24 h for transverse compression, whereas in axial tension the corresponding plateau occurs between 18 and 24 h, and is less expressed. These approximately constant stresses in region II for both deformation states were additionally confirmed by a statistical analysis, see Appendix B. Nevertheless, a clear change in the rate at which stress and tangent decay before and after this time span, can be observed. These results indicate that after storing the tissue samples in NaOH-solution for 18 and 21 h, the muscle cells are destroyed, but the ECM is still intact. Fig. 4 shows histological sections of tissue samples treated for 0, 12, and 18 h. In (a), illustrating a histological section of fresh muscle tissue, the typical microstructure consisting of muscle fibres (yellow) surrounded by ECM (red), is observed. In particular, it should be noted here that the boundaries between ECM and muscle fibre are distinct and clearly visible. An analysis of the histological section (fresh tissue) showed that this sample consists of 83.4% muscle fibres and 16.6% ECM. These values are in good agreement with those in the literature [72,73]. After 12 h (b) it can be clearly seen that only distinct muscle fibres are visible and analyses of this tissue showed a distribution of 55.1% fibres and 44.9% ECM. After 18 h (c) almost no muscle fibre components are present. Only a few small yellow areas indicate that fibrous structures are present but dissolved (muscle fiber 21.8% and ECM 78.2%), so that they can no longer transfer loads. The combination of the mechanical and histological results suggests that 18 h represents a good choice for the sought, optimal insertion time. Accordingly, this time span was used to perform the experiments of group G_3.
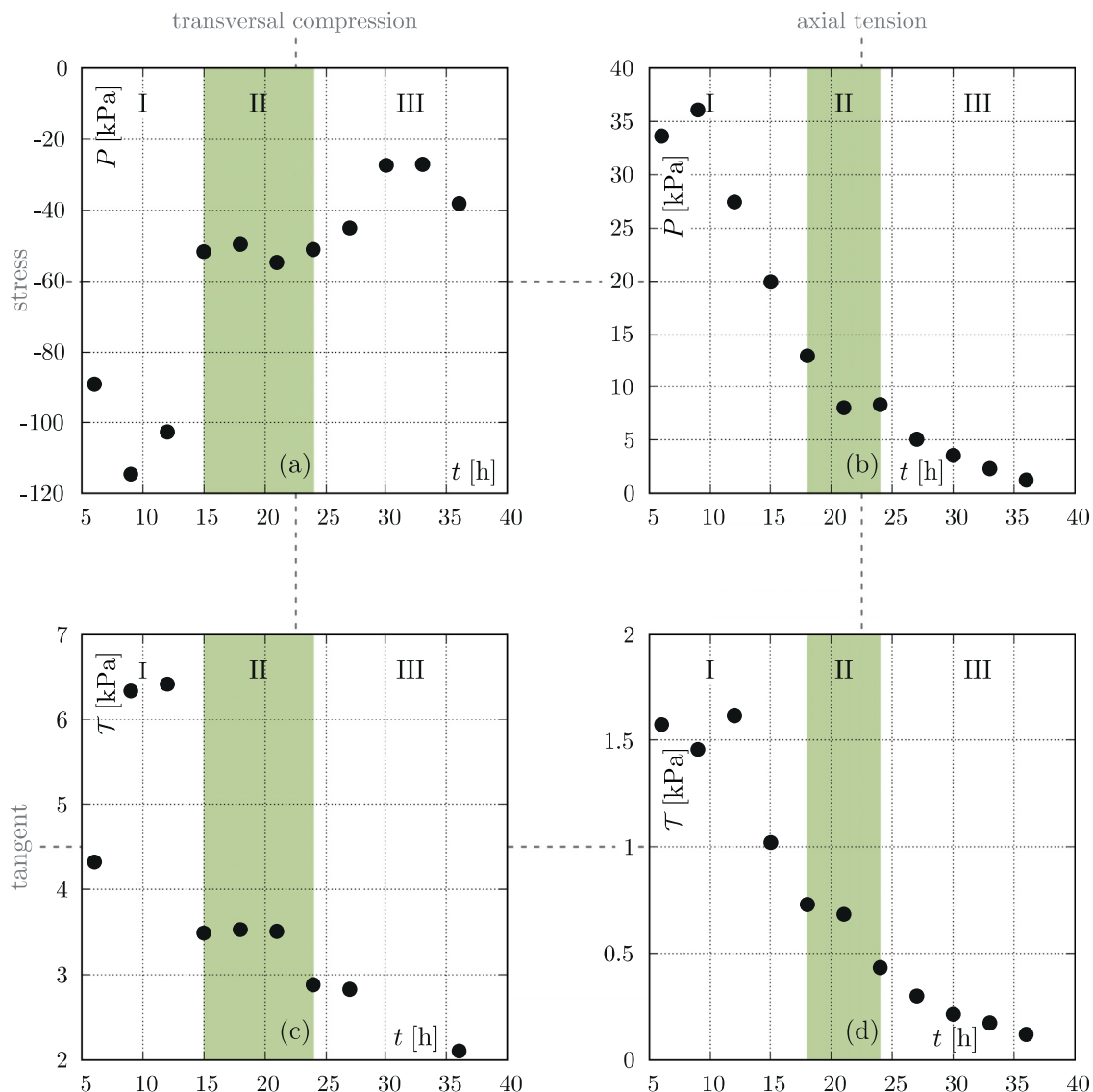
Fig. 3. Transversal compression (left) and axial tension (right) experiments on samples treated with NaOH to determine the optimal insertion time of the tissue.
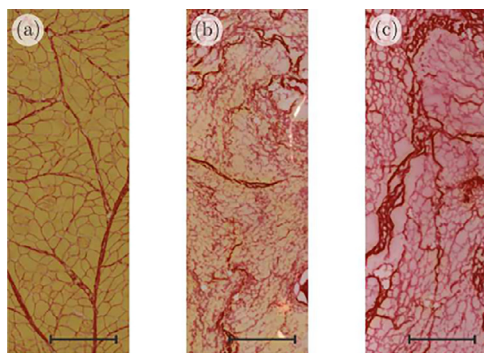

Fig. 4. Histological sectional images of (a) fresh muscle samples, and those inserted for (b) 12 and (c) 18 h, stained with Picro-Sirius red, allowing the differentiation between muscle fibres (yellow) and ECM (red). Scale bars: 500 µm. (For interpretation of the references to colour in this figure legend, the reader is referred to the web version of this article.)

3.3. Axial tension experiments on treated samples

To determine the mechanical characteristics of ECM, muscle samples were tested in axial tension with different angles (0°, 45°, 90°) between the load axis and the previous gross muscle fibre directions. The decellularised samples consist of the collagen scaffold void of the fibres, and hence feature long, oriented pores. Transversal pre-compression by different amounts was applied to collapse these pores and to form an increasingly quasi-planar tissue. To investigate the mechanical anisotropy generated by the porous structure, i.e., at the length scale of the muscle fibres, tensile tests were performed on both the uncompressed (0%) samples, as well as samples pre-compressed to 45% and 90%. The results are shown in Fig. 5. Herein, P is defined as the ratio between force and reference cross-sectional area of the muscle sample before muscle fibre decellularisation, P_{ECM} uses an estimate of the reference cross-sectional area of the ECM.

Independent of the level of pre-compression and the orientation of ECM, all curves are dominated by a non-linear J-shaped material response. Focusing first on the uncompressed samples, see first column, the 0° oriented samples (a) provide the softest response, followed by those with 90° (g) and 45° (d) orientation when comparing the responses up to $\lambda = 1.1$. Similar characteristics, although less pronounced, are observed for pre-compressed samples. Comparing the different levels of pre-compression, similar maximum stress levels are found for the 45% and 90% pre-compressed samples that are higher than those of the uncom-
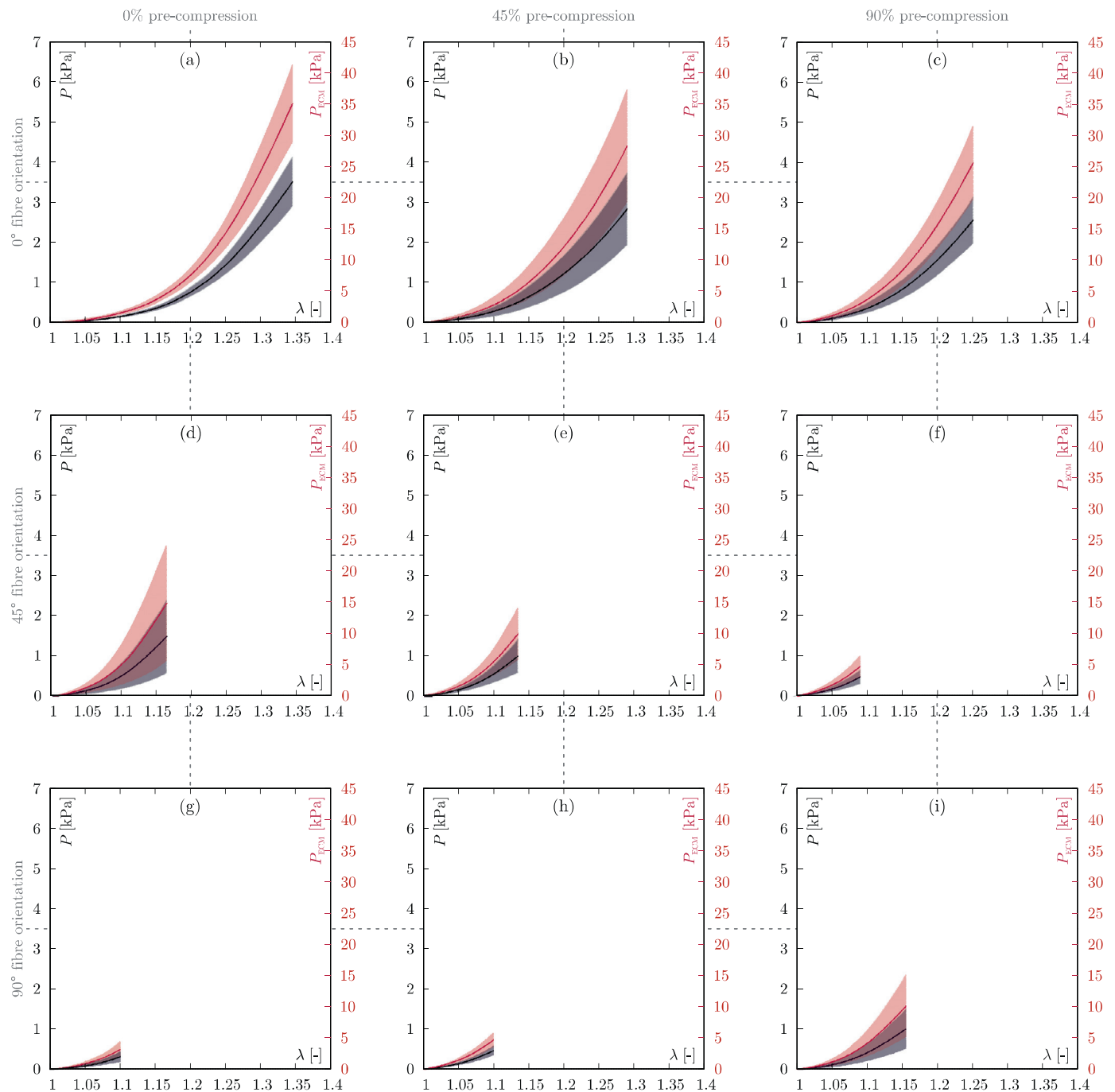
Fig. 5. Orientation- and pre-compression-dependent stress-stretch behaviour of the muscle strips inserted for 18 h in NaOH. Solid curves characterise mean values and shaded areas depict standard deviations. While black curves (mean) and areas (standard deviation) concern to P and red ones belong to P_{ECM}. Note, the unprocessed raw data can be found in the supplementary material, see Section 6. (For interpretation of the references to colour in this figure legend, the reader is referred to the web version of this article.)

pressed samples of the identical fibre orientation group. This can also be seen in Table 4, where the secant stiffnesses are determined based on the stress and stretch values at $\lambda = 1$ and $\lambda = 1.09$. Using Mann–Whitney U-tests for the differently pre-compressed samples (0%, 45%, and 90%), see Section 2.7, it is shown that as the compression level increases, the significant differences between the orientation dependent stress-stretch behaviours are reduced from 100% (0% pre-compression) to approximately 30% (90% pre-compression), indicating a reduction of the tissue's anisotropy level.

The maximum stresses and stretches, indicating the elastic range of the stress-stretch relations, in the form of mean values and standard deviations are summarised in Table 4. As can be seen in Fig. 5, the stress-stretch relations generally feature the strong non-linear behaviour observed for the untreated samples, see Fig. 2. Furthermore, independent of the fibre orientation, the λ_{max} decreases with increasing level of pre-compression. Except for the 90% compression case, the stresses decrease with increasing angle. Noteworthy, λ_{max} is for all 0° samples approximately $\lambda = 1.4$ and for all other samples (45° and 90°) $\lambda = 1.2$.

Table 4

Mean and standard deviation of maximum stress and stretch indicating the end of the elastic range in dependence on the ECM orientation and pre-compression level as well as the secant stiffnesses $K_{\lambda=1.09}$, evaluated at the stretch value $\lambda = 1.09$.

pre-compression	0%			45%			90%		
fibre orientation	0°	45°	90°	0°	45°	90°	0°	45°	90°
$P_{\max}$ [kPa]	4.7 ± 1.1	4.0 ± 1.6	2.1 ± 2.9	6.1 ± 1.5	2.1 ± 1.4	1.6 ± 0.9	5.2 ± 2.2	2.8 ± 2.4	1.4 ± 0.7
$P_{\mathrm{ECM.max}}$ [kPa]	47.5 ± 10.7	40.4 ± 15.8	21.5 ± 29.3	60.6 ± 14.8	21.3 ± 13.6	15.9 ± 8.8	52.4 ± 21.5	28.2 ± 24.4	14.1 ± 6.9
$\lambda_{\max}$ []	1.4 ± 0.0	1.3 ± 0.1	1.2 ± 0.1	1.4 ± 0.1	1.2 ± 0.1	1.2 ± 0.0	1.4 ± 0.1	1.2 ± 0.1	1.2 ± 0.0
$K_{\lambda=1.09}$ [kPa]	1.4	4.4	2.9	2.6	4.9	4.3	3.4	5.3	3.8

Table 5

Mean and standard deviation of the identified factors f.

	0°	45°	90°
0%	1.03 ± 0.17	1.52 ± 0.98	1.12 ± 0.34
45%	1.22 ± 0.72	1.20 ± 0.61	1.06 ± 0.24
90%	1.06 ± 0.29	1.15 ± 0.42	1.18 ± 0.40

3.4. Superposability of fibre and ECM responses

The mean response of skeletal muscle tissue composed of the individual responses of the single components based on a rule of mixture ($\phi = 0.1$) shows large differences to the tensile response of fresh muscle samples as shown in Figure 6 (a). The figure shows two representations of the composite and tissue stresses, once with a pre-load of 0.2 kPa (corresponding to 3 mN) and with a pre-load of 0.7 kPa (corresponding to 30 mN). To emphasise this, the tare load is not subtracted but appears as an offset of the ordinate. Figure 6 (b) provides the longitudinal stretch λ_{MF} that a muscle fibre should experience within the tissue so that the calculated composite response agrees with that of the fresh tissue. Despite all experimental uncertainties and assumptions, these results indicate that the 'true' stretch of the muscle fibres within the tissue is smaller than the tissue stretch, which indicates that the tissue stretch is not directly transferred to the components. The repeated analysis for ECM fractions ϕ of 5% and 15% does not reveal qualitative changes of this result but merely amplifies or attenuates the effect.

3.5. Normalised mean response

Depending on the muscle, but also on the position within a muscle at which the tissue sample is taken, the ECM can vary considerably. We hypothesised that the stress scales linearly with the fraction of ECM and accordingly that a linear scaling factor could be used to collapse the specimen-specific response curves. The original and collapsed curves are shown in Fig. 7, the statistics of the corresponding factors f are summarised in Table 5.

4. Discussion

4.1. Stress-stretch response

In order to characterise the mechanical properties of the ECM in muscle tissue, and to be able to relate them to intact muscle tissue, transverse compression and axial tensile tests were conducted with fresh and NaOH-treated muscle tissue. In addition to single investigations on cadaveric tissue e.g. [44–46,49], experiments hitherto have nearly exclusively been performed on intact tissue. Most of these investigations were performed as axial tension [33,35,36,38,41–47,49,50,74–77] and compression experiments [29–32,34,36–40,48,76]. Muscle tissue from various species, including chicken [38], cattle [29,75,77], rodents [33,41,43,47,50,74], pigs [e.g. 34,39,40,48], and human [44–46,49] was mechanically tested.

Prior to mechanical testing, the tissues were subjected to considerably different protocols. E.g., while in some cases the tissue was tested as soon as possible after dissection [e.g. 29,34,39] to be as close as possible to the in-vivo state, in other studies cadaveric tissue was chosen [46,49] or the tissue was frozen before sampling and then thawed again for the actual mechanical testing [e.g. 33,44,45]. Noteworthy, compared to other tissues, the time-point of testing is of particular concern for skeletal muscle, due to changes in muscle fibre properties after death [40]. Another important factor that influences the mechanical material response is the loading rate, which varies in aforementioned studies between 37,800%/s (high speed load as known from impact scenarios [35]) and 0.001%/s (quasi-static loading [37]). Finally, the reference state to which the deformation measures are related significantly influences the shape and range of the stress-stretch curve, the elastic regime and the failure stretch. There are also different approaches to this in the literature. For example, some studies do not specify a pre-load [e.g. 33,50,74], while others choose it arbitrarily [e.g. 44,46,76] or depending on the tissue sample weight [48]. In view of the large differences between preparation and testing protocols, large variations in the results of these studies seem evident in general.

As shown in Fig. 2, the maximum stresses reached at the end of the smallest elastic range, i.e., at stretches of 1.66 (0°), 1.22 (45°), and 1.14 (90°), take values of 38.0 kPa (0°), 10.6 kPa (45°), and 21.9 kPa (90°), respectively. In particular the stretch in direction of the fibres, see (a) and Table 3, feature relatively high values of 1.66 and 1.9, respectively. Although similar values can be found in the literature, e.g. [41] measured a maximum stretch of 1.72 in rats tibialis anterior muscles, such stretches appear to be too high. A possible reason for this could be the initial length of the muscle. Depending on the joint angle, a muscle features a different initial length in the body, see e.g. [78,79]. In the present study, no attention was paid to the joint angle during dissection, so that different initial lengths were not considered in the present study.

Evaluating the stresses at a smaller stretch value of 1.14 for comparison, the material response of the 0° oriented samples (a) provides the softest response, followed by those with 45° (b) and 90° (c) orientation. Further, statistical investigations reveal significant differences of all stress-stretch relations. Only two studies, by Takaza et al. [48] and Mohammadkhah et al. [38] could be found which present tensile experiments on fresh muscle tissue with angles of 0°, 45° and 90° between loading and fibre direction. The reported nominal stresses at stretches of 1.2, 1.1, and 1.1, for 0°, 45°, and 90° fibre orientation, respectively, vary between 31 to 42 kPa, 41 to 50 kPa, and 23 to 73 kPa. In comparison, in the present study markedly lower stresses of 2 kPa, 3 kPa, and 12 kPa are achieved. While Mohammadkhah et al. [38] investigated chicken pectoralis muscle and mention the variation in tissue structure and composition between species, the difference to the results on porcine longissimus dorsi in Takaza et al. [48] points at either strong variations between muscles of one species or significant influence of the testing protocol. Notwithstanding, when comparing the order of the responses in terms of stiffness, the studies agree in that the
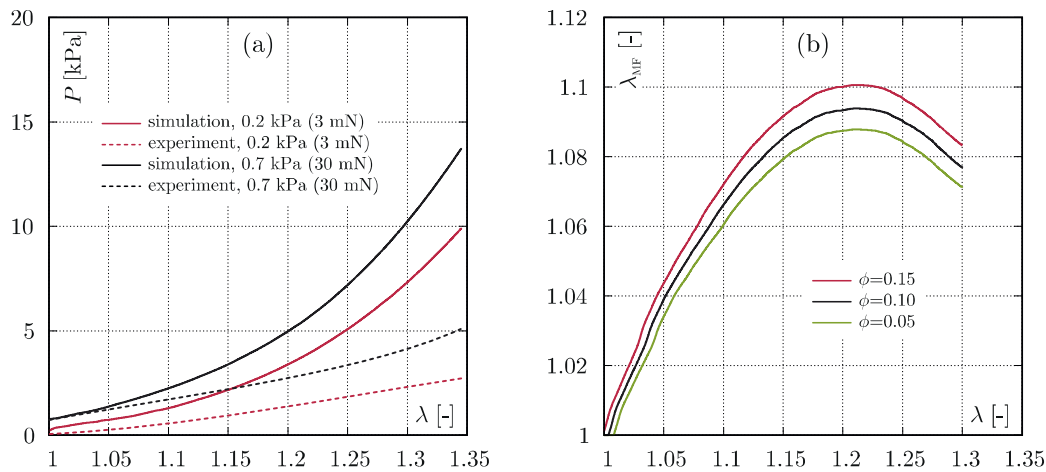
Fig. 6. (a) Difference between experimental tissue response and stress predicted by an additive model combining the individual responses of muscle fibres and ECM. The results are represented for two different pre-loads. (b) Hypothetical stretch of the muscle fibre determined such that the composite model agrees with the tissue response computed for three different ECM fractions ϕ.

tissues feature the softest response in fibre direction ($0°$), followed by the $45°$-direction, and the cross-fibre direction ($90°$) was associated with the highest stresses. Vice-versa, the chicken muscle tissue [38] revealed the stiffest response in the $45°$ direction, while the fibre direction still provided the softest response. Interestingly, this order is also observed in the NaOH-treated, i.e., the ECM-only samples presented in the current study.

4.2. Mechanical characterisation of decellularised samples

A main goal of the present study was the determination of a protocol to prepare samples of skeletal muscle ECM based on tissue decellularisation with caustic soda. Based on the mechanical response of samples treated with NaOH for different amounts of time, see Fig. 3, 18 h was identified as an optimal insertion time, because after this time a time window of several hours was found during which the parameters chosen to characterise the mechanical response remained fairly constant, after a more rapid change before. The change of both the compressive and tensile responses with increasing insertion time could be separated into three phases, see Fig. 3, with changing properties in phases I and III, and relatively stable behaviour in phase II. These findings can be interpreted as follows: In the first phase I the tissue response is close to that of intact tissues, indicated by high stresses. In the second phase II, the muscle cells are destroyed and the intercellular fluid is expelled from the tissue upon mechanical load. In the third phase III, also the ECM looses integrity, so that the stress drops significantly. Histology, cf. Fig. 4, supported these interpretations in that after 18 h the muscle cells were completely dissolved but the ECM was barely affected, when compared to longer insertion times. Based on this result, samples consisting only of ECM were generated and subjected to directional tensile experiments, see Fig. 5. Their systematic testing served to determine the direction-dependent mechanical properties of the ECM in terms of the non-linear stress response in the elastic range, cf. Fig. 5. While at a stretch of 1.1 the responses of $0°$, $45°$, and $90°$ differ moderately, the elastic range reduces markedly from 1.35 to 1.1. The smaller elastic range observed in $90°$ samples, compared to $0°$ ones, suggests that damage in the ECM, e.g., separation of the tissue between fibres and ECM or within the ECM layers, occurs earlier than damage or failure along the muscle fibres. This result is in accordance with observations made by Takaza et al. [48], who report much smaller failure stretches in porcine muscle across than along muscle fibres. Furthermore, the effect of pre-compression

(0%, 45%, 90%) to compact the ECM on the tensile mechanical behaviour was investigated. After decellularisation the samples consist of a hollow structure pervaded by the channels that remain of the dissolved muscle fibres. The thus generated obvious difference between longitudinal and transversal architecture leads to a direction-dependent response of the samples in the tensile tests (0% compression). When transversely compressing the samples by 45% and 90%, the walls of the 'honey-combs', were increasingly forced into one plane, so that the strong structural difference at the length scale of fibres between longitudinal and transverse directions decreases. The data reported in Fig. 5, and the corresponding statistical analysis clearly indicate that this operation also reduces the observed anisotropy in the stress-strain behaviour. We remark, however, that the collagenous networks that form the walls of the endo- and perimysial channels generally feature non-uniform distributions of collagen fibres, see e.g. [11,80], so that anisotropy generated on the length scale of collagen fibres is expected to persist. Overall, with the exception of the $90°$ oriented samples, it was found that with increasing pre-compression, the elastic range, i.e., the maximum stretches are reduced with simultaneous reduction of the maximum stresses, which indicates that damaging mechanism might take place caused by the strong degree of lateral compression, that reduce the overall extensibility of the samples.

So far, there are only few studies in the literature that determine mechanical properties of the ECM in skeletal muscle tissue using indirect [52] or direct measurements [61]. To indirectly determine the mechanical properties of the ECM in murine muscle, Meyer and Lieber [52] measured individual muscle fibres without ECM, muscle fibre bundles including ECM, and muscle fibre bundles without ECM. It was found that isolated single muscle fibres show a linear stress-strain behaviour, whereas the stress strain behaviour of muscle fibre bundles is clearly non-linear. These findings suggested that the ECM as a material is much stiffer than the muscle fibres and behaves in a highly non-linear manner [11]. The much higher material stiffness is also confirmed by our results in Fig. 5(a), that shows that the ECM reaches stresses P_{ECM} of several tens of kilopascals at $\lambda = 1.35$, which is in the order five times more than the corresponding stresses that were observed in a previous study on muscle fibres [69]. When relating the forces of ECM and fibres to the muscle fibre cross-section instead, the ECM stress contribution P becomes comparable in terms of order of magnitude, and even smaller than that muscle fibres. Controversial results also exist with regard to the non-linearity of the fibre response, since the majority of studies on muscle fibres docu-
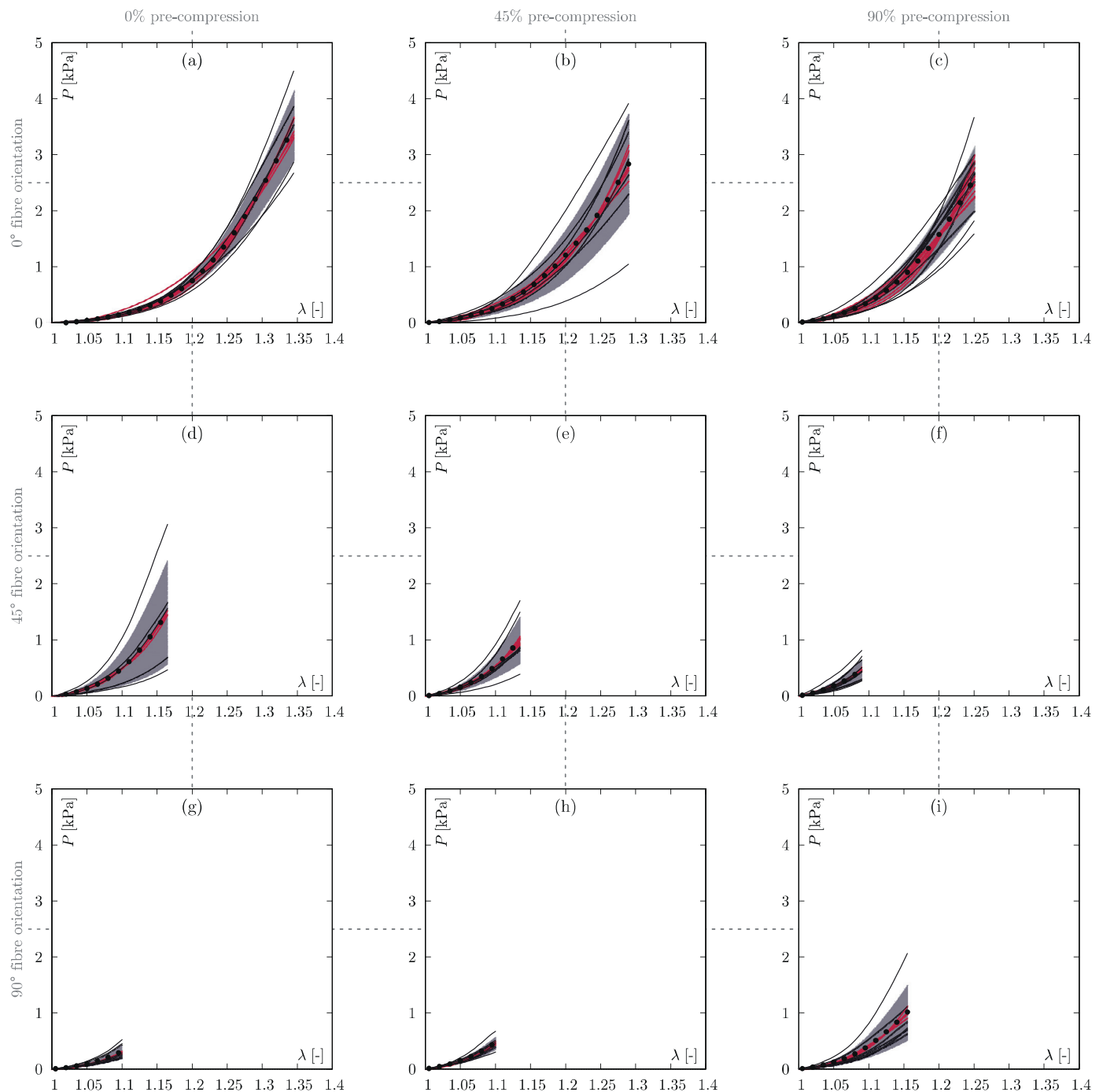
Fig. 7. Orientation- and pre-compression-dependent mean stress-stretch relations: Black curves present mechanical responses of single tension experiments. From these mean relations (black dots) and standard deviations (grey shaded areas) are determined. Red curves illustrate stress-stretch relations of single tension experiments adjusted by a numerically identified factor f to fit best the mean stress-stretch responses. (For interpretation of the references to colour in this figure legend, the reader is referred to the web version of this article.)

ment a strongly non-linear material behaviour, as summarised in Böl et al. [69]. The questions which part of the muscle tissue - fibre or ECM - contribute to the non-linear stress-strain characteristics and to which extent has therefore not conclusively been answered and may strongly depend on the species and muscle type, as suggested by other studies that compare the responses of isolated fibres and fibre bundles [53–55]. Gillies et al. [61] proposed a protocol for decellularisation of muscle tissue, tested bundles of endomysial sheaths and compared them to fibre bundles from untreated muscle of mice. The outcome of this direct analysis, that is in general agreement with our results, suggested that decellu-

larisation does not change the characteristics of the mechanical response, thus providing support for the concept that ECM is main load bearing element in skeletal muscle [61]. However, Gillies et al. [61] also point at the problematic definition of strain due to ambiguity in the definition of a reference state in mechanical testing.

4.3. Implications for mechanical models of skeletal muscle tissue

It is known that the essential mechanical function of the ECM is the connection of the muscle fibres [61,81] and plays a dominating role in the mechanical response of skeletal muscle tissue [52].
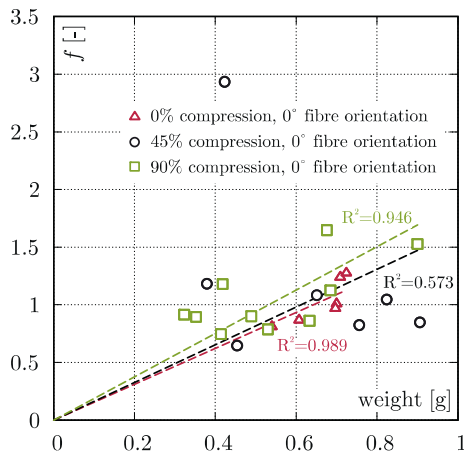
Fig. 8. The factor f plotted against the weight of the tissue samples for compression levels 0%, 45%, and 90% and the fibre direction of $0°$

The varying amount of ECM in different samples of skeletal muscle tissue will cause differences in the tissue response, and thus contribute to the large experimental variability in both untreated and treated muscle tissue samples, see Figs. 2 and 5. Provided that the ECM responds with a characteristic response, i.e., disregarding the variations in the structure and material properties of the ECM, the force generated by decellularised samples should thus scale with the amount of ECM. We therefore tested whether a linear factor f would be sufficient to collapse each response curve onto the mean curve, i.e., to account for the variability between samples [70,71]. The good agreement of the collapsed curves in Fig. 7 supports this idea. For samples tested along the fascicles ($0°$), one would expect that more ECM and thus a higher weight of the sample would lead to more ECM loaded in parallel, and thus give rise to a linear relationship between sample weight and f. At least for the uncompressed samples, the trend and coefficient of determination are in favour of this argument, while for 90% and, particularly, 45% compressed samples such a simple model does not apply, see Fig. 8.

Even if the relation between f and the ECM fraction remains unknown, the observed property, that the response of an individual sample is captured by a multiple of a master curve given by the mean response, is a clear advantage in modelling: The typically large set of material parameters characterising the non-linear response can be fixed while the variability of the response can be captured through varying a linear factor. Moreover, as a result of this linearity the variability in the response is completely described by the statistics of the factor f.

The here presented data presents the first comprehensive data set on the mechanical properties of isolated skeletal muscle ECM. This information provides a hitherto missing piece of information for the development of modelling approaches to analyse and predict the response on skeletal muscle tissue in consideration of its microstructure either in form of idealised constitutive models [e.g. 82–84] or detailed computational models [e.g. 66,85,86]. The information of such models through the component-specific data, however, poses a number of challenges. The approximately unidirectional alignment of muscle fibres within the ECM might suggests that the characteristic stress responses of muscle fibres and ECM sum up to the tissue response, assuming that they act in parallel when the tissue is stretched along the muscle fibre direction. Our preliminary analysis displayed in Fig. 6 cannot entirely exclude that such a superposition would generally be possible. However, the – probably too simplistic – prediction of the tissue response based on the specifically chosen reference states of fibres and ECM, and the assumption that their strain coincides with tissue strain, fails.

The first issue (i) relates to the question of the common reference state, in particular whether the unloaded states of muscle tissue as a whole, muscle fibres, and decellularised ECM coincide. It is known that the definition of a reference state in tensile experiments is difficult for very soft biological tissues, since even tiny loads can cause significant deformations, see e.g. [87,88]. In fact, in their study on decellularised muscle Gillies et al. [61] point at this problematic definition of strain due to ambiguity in the definition of a reference state in mechanical testing. When the response curves of components are superimposed to represent a composite, differences in their seemingly undeformed states can become consequential. Noteworthy, for skeletal muscle tissue, the harmonisation of the reference states of single fibres and muscle tissue through an analysis of the sarcomere lengths could serve as an alternative to define a reliable reference state, even if this might not be possible on a sample specific basis. The second point (ii) concerns the potential deviations and relation between the strains observed on the tissue-scale, compared to the deformations undergone by the single components within the tissue. The reasons for these differences are manifold, including a non-homogeneous disposition of the components, structural effects such as alignment or straightening of curved fibres, and the complex transfer of loads between the components, that are all absent when testing the components individually. We illustrated this in Fig. 6(b), where the hypothetical effective stretch of the muscle fibre λ_{MF} computed such that the composite model matches the tissue response is consistently smaller than the tissue stretch λ, and even shows non-monotonic behaviour. Clearly these curves are strongly affected by the selection of the state at which fibres and ECM are composed; choosing a higher reference stress for the ECM, for example, would even reduce the muscle fibre stretch required to match the tissue response. Given the arbitrary choice of the threshold stresses, the curves in Fig. 6(b) are therefore unlikely to be representative of the muscle fibre stretch in the real tissue both in shape and magnitude. However, the theoretical analysis highlights that differences between component and tissue strains may exist and be non-uniform, depending on the non-linearities in the behaviour of ECM and muscle fibres. Similar effects of "stretch amplification" and "attenuation" [89] over the scales have been reported for other musculoskeletal tissues [e.g. 89,90].

4.4. Limitations

As we did not succeed in adding reliably trackable markers on the surface of the decellularised samples, all stretches presented in this study were calculated based on the crosshead travel, i.e., the displacement output of the testing machine. This also concerns the data on fresh muscle, even though these global stretches can differ from the local ones measured on the sample's surface by means of optical methods, especially for soft materials such as muscle tissue, see e.g. Takaza et al. [48]. Although we could not detect any slippage of our samples out of the clamps, the low aspect ratio and tissue heterogeneity might have caused deviations between the global estimate and the actual local state of deformation. This deviation might partially explain the relatively large differences in the stretch ranges between our study and the one by Takaza et al. [48], which reports local stretches. Finally, studies reveal that the treatment of muscle tissue samples with NaOH to isolate ECM not only digests the muscle cell structure but also can deplete the ground matrix of the ECM, composed of proteoglycans or even damage collagenous network depending on concentration and temperature [4,8]. Fixation agents have been used to stabilise the ECM during digestion in order to study its structure [8]. For the mechanical characterisation of ECM, fixation is clearly not possible due to its potentially strong impact on mechanical properties. Hence, the response to lateral compression was used as the only

indicator for removal of the muscle fibres, and based on this, it is assumed that the NaOH concentration employed was high enough to digest muscle cells, however, its potential effect on the ECM ground matrix remains unverified in this work.

5. Conclusions

The present work presents a simple protocol for isolating and testing endo- and perimysial ECM of skeletal muscle tissue by decellularisation in caustic soda solution and subsequent mechanical characterisation. It was shown through mechanical indicators and supported by histology that for the porcine muscle considered here, an optimal time window of several hours exists at around 18 h, in which the storage in the decellularising solution caused a complete destruction and removal of the muscle fibres while leaving the collagenous ECM largely intact and mechanically functional. Mechanical characterisation of the ECM in axial tension tests revealed strongly non-linear, direction-dependent, i.e., anisotropic properties. A prominent difference between the responses of intact muscle and ECM is the order between the stress responses. Surprisingly, ECM samples tested at an angle of 45° with respect to the direction of the muscle fibres provided the stiffest response, whereas for intact muscle the cross-fibre direction is the stiffest. Lateral pre-compression, through which the decellularised sheaths of ECM were compacted to flat membrane-like structures, had a moderate effect on the stress-strain curves but reduced the width of the elastic range of the response. Despite the generally observed large variability in the experimental data, the response curves of ECM samples tested at the same orientation and with equal level of pre-compression could be fairly collapsed onto the mean curve by a single scalar factor. Thus suggesting that the sample-specific amount of ECM is a major contributor to the experimental scatter in the mechanical response. Altogether, the proposed method and the corresponding results help filling the gap of information that exists on the mechanical properties of the individual components of skeletal muscle tissue, and in particular, they can provide key information necessary to develop and parametrise micromechanical models of muscle tissue. At the same time the findings pose new questions, e.g., on the common reference state among the components and the composite tissue. Applying, elaborating and adapting the presented techniques will contribute towards addressing these questions and understanding the complex mechanisms that govern the mechanics of skeletal muscle.

Declaration of Competing Interest

The authors declare that they have no known competing financial interests or personal relationships that could have appeared to influence the work reported in this paper.

Acknowledgements

Appendix A. Picro–Sirius red staining protocol for skeletal muscle tissue

1. Freeze the sample for 20 s in an isopentane bath cooled with liquid nitrogen.
2. Store the frozen sample wrapped in aluminum foil at −80 °C until use.
3. Cut sections 14 μm thick at −14 °C and put onto glass microscope slide.
4. Allow sections to precipitate at room temperature until the next day.
5. Fix sections with Picro–Formalin for 5 min.
6. Rinse sections under gently running water for 10 min.
7. Stain sections with Picro–Sirius red solution for 60 min.
8. Rinse sections with acidified water for 2 min twice.
9. Rinse sections with distilled water for 1 min.
10. Dehydrate sections with ethanol 96% for 1 min.
11. Dehydrate sections with isopropanol for 1 min twice.
12. Clear sections with Roti–Histol for 2 min twice.
13. Cover sections with a mounting medium.

Appendix B. Statistical analyses for the determination of the optimal insertion time $t^* = 18$ h

Within the present study transverse compression and tension experiments were carried out to determine the optimum insertion time t^*. For both deformation states, four to eight samples were tested for each insertion time (ranging between 6 to 30 h, see also Table 2). The stress values were statistically evaluated with unpaired Mann–Whitney U-tests to check the stress value at a specific decellularisation duration and the one at the optimal insertion time. Thereby, the optimal insertion time of 18 h was selected based on the histological examinations, see Fig. 4. The p-values between 12 and 24 h suggest less statistical difference for insertion times between 12 and 24 h for the compression tests, and between 15 and 18 h for the tensile tests, see underlined numbers in Table 6. Due to the very large decrease in stress between the two insertion times of 15 and 18 h by 54.5% from 32.3 ± 17.7 to 20.9 ± 4.6 kPa and under additional consideration of the histological results, the optimal insertion was finally defined to be $t^* = 18$ h.

Table 6
p-values for the hypothesis that the stress at a given insertion time feature not statistical difference to the one after $t^* = 18$ h in transverse compression and uniaxial tension. Underlined numbers indicate $p > 0.05$.

Groups [h]	Transversal compression	Uniaxial tension
6	0.0283	0.0002
9	0.0205	0.0002
12	0.4634	0.0070
15	0.4908	0.2786
21	0.0541	0.0593
24	0.2786	0.2345
27	0.0281	0.0037
30	0.0016	0.0007

Supplementary material

Supplementary material associated with this article can be found, in the online version, at doi:10.1016/j.actbio.2020.12.050.

Supplementary material in form of unprocessed raw data (stress-stress relations) of Figs. 2 and 5 can be found in online version of the article.

References

[1] A. Listrat, B. Picard, Y. Geay, Age-related changes and location of type I, III, IV, V and VI collagens during development of four foetal skeletal muscles of double-muscled and normal bovine animals, Tissue Cell 31 (1) (1999) 17–27.

[2] A. Listrat, C. Lethias, J.F. Hocquette, G. Renand, F. Ménissier, Y. Geay, B. Picard, Age-related changes and location of types I, III, XII and XIV collagen during development of skeletal muscles from genetically different animal, Histochem. J. 32 (6) (2000) 349–356.

[3] P.P. Purslow, Muscle fascia and force transmission, J. Bodyw. Mov. Ther. 14 (4) (2010) 411–417.

[4] P.P. Purslow, J.A. Trotter, The morphology and mechanical properties of endomysium in series-fibred muscles: variations with muscle length, J. Muscle Res. Cell Motil. 15 (3) (1994) 299–308.

[5] T. Nishimura, A. Hattori, K. Takahashi, Ultrastructure of the intramuscular connective tissue in bovine skeletal muscle, Cells Tissues Organs 151 (4) (1994) 250–257.

[6] T. Nishimura, K. Ojima, A. Liu, A. Hattori, K. Takahashi, Structural changes in the intramuscular connective tissue during development of bovine semitendinosus muscle, Tissue Cell 28 (5) (1996) 527–536.

[7] J.A. Trotter, Interfiber tension transmission in series-fibered muscles of the cat hindlimb, J. Morphol. 206 (3) (1990) 351–361.

[8] E. Passerieux, R. Rossignol, T. Letellier, J.P. Delage, Physical continuity of the perimysium from myofibers to tendons: involvement in lateral force transmission in skeletal muscle, J. Struct. Biol. 159 (1) (2007) 19–28.

[9] T.A. Järvinen, L. Józsa, P. Kannus, T.L. Järvinen, M. Järvinen, Organization and distribution of intramuscular connective tissue in normal and immobilized skeletal muscles, J. Muscle Res. Cell Motil. 23 (3) (2002) 245–254.

[10] E. Passerieux, R. Rossignol, A. Chopard, A. Carnino, J.F. Marini, T. Letellier, J.P. Delage, Structural organization of the perimysium in bovine skeletal muscle: Junctional plates and associated intracellular subdomains, J. Struct. Biol. 154 (2) (2006) 206–216.

[11] A.R. Gillies, R.L. Lieber, Structure and function of the skeletal muscle extracellular matrix, Muscle Nerve 44 (3) (2011) 318–331.

[12] P.A. Huijing, Epimuscular myofascial force transmission between antagonistic and synergistic muscles can explain movement limitation in spastic paresis, J. Electromyogr. Kinesiol. 17 (6) (2007) 708–724.

[13] M. Kjaer, Role of extracellular matrix in adaptation of tendon and skeletal muscle to mechanical loading, Physiol. Rev. 84 (2) (2004) 649–698.

[14] S. Thorsteinsdóttir, M. Deries, A.S. Cachaço, F. Bajanca, The extracellular matrix dimension of skeletal muscle development, Dev. Biol. 354 (2) (2011) 191–207.

[15] K. Thomas, A.J. Engler, G.A. Meyer, Extracellular matrix regulation in the muscle satellite cell niche, Connect. Tissue Res. 56 (1) (2015) 1–8.

[16] K. Grzelkowska-Kowalczyk, The importance of extracellular matrix in skeletal muscle development and function, in: F. Travascio (Ed.), Composition and Function of the Extracellular Matrix in the Human Body, InTechOpen, Rijeka and Kroatien, 2016, pp. 3–24.

[17] K. Ahmad, J.-J. Lee, J.S. Moon, S.Y. Park, I. Choi, Multifaceted interweaving between extracellular matrix, insulin resistance, and skeletal muscle, Cells 7 (10) (2018) 148.

[18] N.K. Karamanos, A.D. Theocharis, T. Neill, R.V. Iozzo, Matrix modeling and remodeling: a biological interplay regulating tissue homeostasis and diseases, Matrix Biol. 75 (1) (2019) 1–11.

[19] A.D. Theocharis, N.K. Karamanos, Proteoglycans remodeling in cancer: underlying molecular mechanisms, Matrix Biol. 75 (1) (2019) 220–259.

[20] I. Riederer, A.C. Bonomo, V. Mouly, W. Savino, Laminin therapy for the promotion of muscle regeneration, FEBS Lett. 589 (22) (2015) 3449–3453.

[21] A.R. Gillies, M.A. Chapman, E.A. Bushong, T.J. Deerinck, M.H. Ellisman, R.L. Lieber, High resolution three-dimensional reconstruction of fibrotic skeletal muscle extracellular matrix, J. Physiol. 595 (4) (2017) 1159–1171.

[22] P.M. van Ry, T.M. Fontelonga, P. Barraza-Flores, A. Sarathy, A.M. Nunes, D.J. Burkin, ECM–related myopathies and muscular dystrophies: pros and cons of protein therapies, Compr. Physiol. 7 (4) (2017) 1519–1536.

[23] H.S. Sonbol, Extracellular matrix remodeling in human disease, J. Microsc. Ultrast. 6 (3) (2018) 123–128.

[24] T.J. McKee, G. Perlman, M. Morris, S.V. Komarova, Extracellular matrix composition of connective tissues: a systematic review and meta-analysis, Sci. Rep. 9 (1) (2019) 1–15.

[25] J.T. Oxford, J.C. Reeck, M.J. Hardy (Eds.), Extracellular Matrix in Development and Disease, MDPI, Basel, Schweiz, 2019.

[26] A.D. Theocharis, D. Manou, N.K. Karamanos, The extracellular matrix as a multitasking player in disease, FEBS J. 286 (15) (2019) 2830–2869.

[27] M. Tabebordbar, E.T. Wang, A.J. Wagers, Skeletal muscle degenerative diseases and strategies for therapeutic muscle repair, Annu. Rev. Pathol. 8 (1) (2013) 441–475.

[28] K. Mukund, S. Subramaniam, Skeletal muscle: a review of molecular structure and function, in health and disease, Wiley Interdiscip. Rev. 12 (1) (2020) e1462.

[29] M. van Loocke, C.G. Lyons, C.K. Simms, A validated model of passive muscle in compression, J. Biomech. 39 (16) (2006) 2999–3009.

[30] M. van Loocke, C.G. Lyons, C.K. Simms, Viscoelastic properties of passive skeletal muscle in compression: stress-relaxation behaviour and constitutive modelling, J. Biomech. 41 (7) (2008) 1555–1566.

[31] M. van Loocke, C.K. Simms, C.G. Lyons, Viscoelastic properties of passive skeletal muscle in compression—cyclic behaviour, J. Biomech. 42 (8) (2009) 1038–1048.

[32] A. Chawla, S. Mukherjee, B. Karthikeyan, Characterization of human passive muscles for impact loads using genetic algorithm and inverse finite element methods, Biomech. Model. Mechanobiol. 8 (1) (2009) 67–76.

[33] D.A. Morrow, T.L.H. Donahue, G.M. Odegard, K.R. Kaufman, Transversely isotropic tensile material properties of skeletal muscle tissue, J. Mech. Behav. Biomed. Mater. 3 (1) (2010) 124–129.

[34] M. Böl, R. Kruse, A.E. Ehret, K. Leichsenring, T. Siebert, Compressive properties of passive skeletal muscle—the impact of precise sample geometry on parameter identification in inverse finite element analysis, J. Biomech. 45 (15) (2012) 2673–2679.

[35] M. Takaza, K.M. Moerman, C.K. Simms, Passive skeletal muscle response to impact loading: experimental testing and inverse modelling, J. Mech. Behav. Biomed. Mater. 27 (1) (2013) 214–225.

[36] M. Takaza, G.M. Cooney, G. McManus, P. Stafford, C.K. Simms, Assessing the microstructural response to applied deformation in porcine passive skeletal muscle, J. Mech. Behav. Biomed. Mater. 40 (1) (2014) 115–126.

[37] R. Pietsch, B.B. Wheatley, T.L.H. Donahue, R. Gilbrech, R. Prabhu, J. Liao, L.N. Williams, Anisotropic compressive properties of passive porcine muscle tissue, J. Biomech. Eng. 136 (11) (2014) 111003.

[38] M. Mohammadkhah, P. Murphy, C.K. Simms, The in vitro passive elastic response of chicken pectoralis muscle to applied tensile and compressive deformation, J. Mech. Behav. Biomed. Mater. 62 (1) (2016) 468–480.

[39] M. Böl, A.E. Ehret, K. Leichsenring, C. Weichert, R. Kruse, On the anisotropy of skeletal muscle tissue under compression, Acta Biomater. 10 (7) (2014) 3225–3234.

[40] M. Böl, K. Leichsenring, M. Ernst, A.E. Ehret, Long-term mechanical behaviour of skeletal muscle tissue in semi-confined compression experiments, J. Mech. Behav. Biomed. Mater. 63 (1) (2016) 115–124.

[41] B. Calvo, A. Ramírez, A. Alonso, J. Grasa, F. Soteras, R. Osta, M.J. Muñoz, Passive nonlinear elastic behaviour of skeletal muscle: experimental results and model formulation, J. Biomech. 43 (2) (2010) 318–325.

[42] X. Nie, J.I. Cheng, W.W. Chen, T. Weerasooriya, Dynamic tensile response of porcine muscle, J. Appl. Mech. 78 (2) (2011) 021009.

[43] B. Hernández, E. Peña, G. Pascual, M. Rodríguez, B. Calvo, M. Doblaré, J.M. Bellón, Mechanical and histological characterization of the abdominal muscle. a previous step to modelling hernia surgery, J. Mech. Behav. Biomed. Mater. 4 (3) (2011) 392–404.

[44] L.L. Gras, D. Mitton, P. Viot, S. Laporte, Hyper-elastic properties of the human sternocleidomastoideus muscle in tension, J. Mech. Behav. Biomed. Mater. 15 (1) (2012) 131–140.

[45] L.L. Gras, D. Mitton, P. Viot, S. Laporte, Viscoelastic properties of the human sternocleidomastoideus muscle of aged women in relaxation, J. Mech. Behav. Biomed. Mater. 27 (1) (2013) 77–83.

[46] L.L. Gras, S. Laporte, P. Viot, D. Mitton, Experimental characterization of post rigor mortis human muscle subjected to small tensile strains and application of a simple hyper-viscoelastic model, Proc. Inst. Mech. Eng. Part H 228 (10) (2014) 1059–1068.

[47] A.C. Abraham, K.R. Kaufman, T.L.H. Donahue, Phenomenological consequences of sectioning and bathing on passive muscle mechanics of the New Zealand white rabbit tibialis anterior, J. Mech. Behav. Biomed. Mater. 17 (1) (2013) 290–295.

[48] M. Takaza, K.M. Moerman, J. Gindre, G. Lyons, C.K. Simms, The anisotropic mechanical behaviour of passive skeletal muscle tissue subjected to large tensile strain, J. Mech. Behav. Biomed. Mater. 17 (1) (2013) 209–220.

[49] A.S. Nagle, M.A. Barker, S.D. Kleeman, B. Haridas, T.D. Mast, Passive biomechanical properties of human cadaveric levator ani muscle at low strains, J. Biomech. 47 (2) (2014) 583–586.

[50] B.B. Wheatley, D.A. Morrow, G.M. Odegard, K.R. Kaufman, T.L.H. Donahue, Skeletal muscle tensile strain dependence: hyperviscoelastic nonlinearity, J. Mech. Behav. Biomed. Mater. 53 (1) (2016) 445–454.

[51] M. van Turnhout, G. Peters, A. Stekelenburg, C. Oomens, Passive transverse mechanical properties as a function of temperature of rat skeletal muscle in vitro, Biorheology 42 (3) (2005) 193–207.

[52] G.A. Meyer, R.L. Lieber, Elucidation of extracellular matrix mechanics from muscle fibers and fiber bundles, J. Biomech. 44 (4) (2011) 771–773.

[53] S.H. Brown, J.A. Carr, S.R. Ward, R.L. Lieber, Passive mechanical properties of rat abdominal wall muscles suggest an important role of the extracellular connective tissue matrix, J. Orthop. Res. 30 (8) (2012) 1321–1326.

[54] L.K. Wood, E. Kayupov, J.P. Gumucio, C.L. Mendias, D.R. Claflin, S.V. Brooks, Intrinsic stiffness of extracellular matrix increases with age in skeletal muscles of mice, J. Appl. Physiol. 117 (4) (2014) 363–369.

[55] G. Meyer, R.L. Lieber, Muscle fibers bear a larger fraction of passive muscle tension in frogs compared with mice, J. Exp. Biol. 221 (22) (2018) jeb182089.

[56] H.L. Granzier, T.C. Irving, Passive tension in cardiac muscle: contribution of collagen, titin, microtubules, and intermediate filaments, Biophys. J. 68 (3) (1995) 1027–1044.

[57] S.F. Badylak, D. Taylor, K. Uygun, Whole-organ tissue engineering: decellularization and recellularization of three-dimensional, Annu. Rev. Biomed. Eng. 13 (1) (2011) 27–53.

[58] P.M. Crapo, T.W. Gilbert, S.F. Badylak, An overview of tissue and whole organ decellularization processes, Biomaterials 32 (12) (2011) 3233–3243.

[59] R.H. Fu, Y.C. Wang, S.P. Liu, T.R. Shih, H.L. Lin, Y.M. Chen, J.H. Sung, C.H. Lu, J.R. Wei, Z.W. Wang, S.J. Huang, C.H. Tsai, W.C. Shyu, S.Z. Lin, Decellularization and recellularization technologies in tissue engineering, Cell Transpl. 23 (4-5) (2014) 621–630.

[60] K.H. Hillebrandt, H. Everwien, N. Haep, K. Keshi, J. Pratschke, I.M. Sauer, Strategies based on organ decellularization and recellularization, Transpl. Int. 32 (6) (2019) 571–585.

[61] A.R. Gillies, L.R. Smith, R.L. Lieber, S. Varghese, Method for decellularizing skeletal muscle without detergents or proteolytic enzymes, Tissue Eng. Part C 17 (4) (2011) 383–389.

[62] Y. Gao, T.Y. Kostrominova, J.A. Faulkner, A.S. Wineman, Age-related changes in the mechanical properties of the epimysium in skeletal muscles of rats, J. Biomech. 41 (2) (2008) 465–469.

[63] O. Ohtani, T. Ushiki, T. Taguchi, A. Kikuta, Collagen fibrillar networks as skeletal frameworks: ademonstration by cell-maceration/scanning electron microscope method, Arch. Histol. Cytol. 51 (3) (1988) 249–261.

[64] J.A. Trotter, P.P. Purslow, Functional morphology of the endomysium in series fibered muscles, J. Morphol. 212 (2) (1992) 109–122.

[65] P.P. Purslow, The structure and functional significance of variations in the connective tissue within muscle, Comparat. Biochem. Physiol. Part A 133 (4) (2002) 947–966.

[66] R. Kuravi, K. Leichsenring, M. Böl, A.E. Ehret, 3D finite element models from serial section histology of skeletal muscle tissue—The role of micro-architecture on mechanical behaviour, J. Mech. Behav. Biomed. Mater. 113 (2021) 104109.

[67] M. Böl, A.E. Ehret, K. Leichsenring, M. Ernst, Tissue-scale anisotropy and compressibility of tendon in semi-confined compression tests, J. Biomech. 48 (6) (2015) 1092–1098.

[68] M. Böl, R. Kruse, A.E. Ehret, On a staggered iFEM approach to account for friction in compression testing of soft materials, J. Mech. Behav. Biomed. Mater. 27 (1) (2013) 204–213.

[69] M. Böl, R. Iyer, J. Dittmann, M. Garcés-Schröder, A. Dietzel, Investigating the passive mechanical behaviour of skeletal muscle fibres: micromechanical experiments and bayesian hierarchical modelling, Acta Biomater. 92 (1) (2019) 277–289.

[70] A. Mauri, A.E. Ehret, D.S. de Focatiis, E. Mazza, A model for the compressible, viscoelastic behavior of human amnion addressing tissue variability through a single parameter, Biom. Model. Mechanobiol. 15 (4) (2016) 1005–1017.

[71] K. Bircher, A.E. Ehret, E. Mazza, Mechanical characteristics of bovine Glisson's capsule as a model tissue for soft collagenous membranes, J. Biomech. Eng. 138 (8) (2016).

[72] L.R. Smith, E.R. Barton, Collagen content does not alter the passive mechanical properties of fibrotic skeletal muscle in MDX mice, Am. J. Physiol. Cell Physiol. 306 (10) (2014) C889–C898.

[73] C.L. Dunham, A.M. Chamberlain, G.A. Meyer, S.P. Lake, Muscle does not drive persistent posttraumatic elbow contracture in a rat model, Muscle Nerve 58 (6) (2018) 843–851.

[74] D.A. Morrow, T.L.H. Donahue, G.M. Odegard, K.R. Kaufman (Eds.), Tensile Material Properties of Skeletal Muscle Tissue in Longitudinal and Transverse Directions, 2008.

[75] L. Yoo, H. Kim, V. Gupta, J.L. Demer, Quasilinear viscoelastic behavior of bovine extraocular muscle tissue, Investig. Ophthalmol. Vis. Sci. 50 (8) (2009) 3721–3728.

[76] N. Jalal, M. Zidi, Effect of cryopreservation at $-80\,^\circ$C on visco-hyperelastic properties of skeletal muscle tissue, J. Mech. Behav. Biomed. Mater. 77 (1) (2018) 572–577.

[77] A.A. Yousefi, M.A. Nazari, P. Perrier, M.S. Panahi, Y. Payan, A new model of passive muscle tissue integrating collagen fibers: consequences for muscle behavior analysis, J. Mech. Behav. Biomed. Mater. 88 (1) (2018) 29–40.

[78] M. Böl, K. Leichsenring, C. Weichert, M. Sturmat, P. Schenk, R. Blickhan, T. Siebert, Three-dimensional surface geometries of the rabbit soleus muscle during contraction: input for biomechanical modelling and its validation, Biomech. Model. Mechanobiol. 12 (6) (2013) 1205–1220.

[79] T. Siebert, K. Leichsenring, C. Rode, C. Wick, N. Stutzig, H. Schubert, R. Blickhan, M. Böl, Three-dimensional muscle architecture and comprehensive dynamic properties of rabbit gastrocnemius, plantaris and soleus: input for simulation studies, PLoS One 10 (6) (2015) e0130985.

[80] P.P. Purslow, The extracellular matrix of skeletal and cardiac muscle, in: P. Fratzl (Ed.), Collagen: Structure and Mechanics, Springer US, Boston, MA, 2008, pp. 325–357.

[81] R. Csapo, M. Gumpenberger, B. Wessner, Skeletal muscle extracellular matrix–what do we know about its composition, regulation, and physiological roles? A narrative review, Front. Physiol. 11 (1) (2020) 253.

[82] J. Gindre, M. Takaza, K.M. Moerman, C.K. Simms, A structural model of passive skeletal muscle shows two reinforcement processes in resisting deformation, J. Mech. Behav. Biomed. Mater. 22 (1) (2013) 84–94.

[83] M. Latorre, M. Mohammadkhah, C.K. Simms, F.J. Montáns, A continuum model for tension-compression asymmetry in skeletal muscle, J. Mech. Behav. Biomed. Mater. 77 (1) (2018) 455–460.

[84] C. Bleiler, P.P. Castañeda, O. Röhrle, A microstructurally-based, multi-scale, continuum-mechanical model for the passive behaviour of skeletal muscle tissue, J. Mech. Behav. Biomed. Mater. 97 (1) (2019) 171–186.

[85] K.M. Virgilio, K.S. Martin, S.M. Peirce, S.S. Blemker, Multiscale models of skeletal muscle reveal the complex effects of muscular dystrophy on tissue mechanics and damage susceptibility, Interface Focus 5 (2) (2015) 20140080.

[86] L.A. Spyrou, S. Brisard, K. Danas, Multiscale modeling of skeletal muscle tissues based on analytical and numerical homogenization, J. Mech. Behav. Biomed. Mater. 92 (1) (2019) 97–117.

[87] Z. Gao, J.P. Desai, Estimating zero-strain states of very soft tissue under gravity loading using digital image correlation, Med. Image Anal. 14 (2) (2010) 126–137.

[88] W. Buerzle, E. Mazza, On the deformation behavior of human amnion, J. Biomech. 46 (11) (2013) 1777–1783.

[89] M.L. Upton, C.L. Gilchrist, F. Guilak, L.A. Setton, Transfer of macroscale tissue strain to microscale cell regions in the deformed meniscus, Biophys. J. 95 (4) (2008) 2116–2124.

[90] H.R.C. Screen, D.L. Bader, D.A. Lee, J.C. Shelton, Local strain measurement within tendon, Strain 40 (4) (2004) 157–163.